Arabian Journal of Chemistry (2023) **16**, 104515

King Saud University

Arabian Journal of Chemistry

www.ksu.edu.sa
www.sciencedirect.com

REVIEW ARTICLE

Synthesis of polyaspartic acid-glycidyl adduct and evaluation of its scale inhibition performance and corrosion inhibition capacity for Q235 steel applications

Xinhua Liu [a,*], Yuhua Gao [b], Yongguang Gao [a], Yong Yang [a], Wentao Li [a], Nan Ma [a], Jiaqi Zhao [a]

[a] *Department of Chemistry, Tangshan Normal University, Tangshan 063000, Hebei, China*
[b] *Institute of Energy Resources, Hebei Academy of Sciences, Shijiazhuang 050081, Hebei, China*

Received 10 July 2022; accepted 7 December 2022
Available online 14 December 2022

KEYWORDS

Polyaspartic acid/glycidyl;
Ring-openning graft modification;
Scale and a corrosion inhibitor;
Scale and corrosion inhibition efficiency;
Electrochemical measurement

Abstract In this work, the development of the eco-friendly comprehensive scale and corrosion inhibitor based on green polyaspartic acid (PASP) was presented. In this view, PASPG was prepared by a ring-opening graft modification reaction of polysuccinimide (PSI) with glycidyl. In addition, the molecular structure and the thermal stability of PASPG were characterized by using three different methods (FTIR, ^{1}H NMR, and TGA). PASPG's scale inhibition efficiency and corrosion inhibition efficiency were also evaluated, respectively. More concretely, the scale inhibition efficiency of PASPG achieved 94.6 % and 95.1 % for $CaCO_3$ and $CaSO_4$, respectively. With the aid of the FTIR and SEM measurement techniques, it was found that PASPG could induce the irregular growth of the $CaCO_3$ and $CaSO_4$ morphology and destroy the formation of crystals. On the other hand, the higher corrosion efficiency of 85.17 % was achieved by PASPG in comparison with PASP (72.53 %). PASPG is a mixed inhibitor and the adsorption of PASPG on the Q235 steel surface followed the Langmuir mono-layer adsorption isotherm. The formation of a protective film on the surface of carbon steel was proved by PASPG's adsorption, which increased the resistance to be eroded. Thus, the surface of carbon steel can be effectively protected. The present work provides a simple and effective pathway for the synthesis of high-efficiency green scale and corrosion inhibitor,

* Corresponding author.
E-mail address: hualiyiwang@163.com (X. Liu).
Peer review under responsibility of King Saud University.

Production and hosting by Elsevier

https://doi.org/10.1016/j.arabjc.2022.104515

by introducing a functional group into the PASP chains. The implementation of such type of chemical modification method may also be an effective strategy for improving the efficiency of other polymers green scale and corrosion inhibitors.

1. Introduction

With the rapid development of the economy, the demand for water in industrial production has greatly increased. Therefore, the shortage of water poses serious problems. One effective way to solve this problem is recycling water resources [Chen et al. 2020, Nayunigari et al. 2016]. However, during the recycling process of the cooling water, the concentration of Ca^{2+} is gradually increased and a massive scale will be formed. The scale will be then attached to the surface of the pipeline or the equipment of the cooling water system, resulting in the reduction of the efficiency of the heat transfer procedure and the acceleration of the pipeline corrosion [Chaussemier et al. 2015, Al-Roomi and Hussain. 2015, Guo et al. 2021].

Along these lines, to inhibit the formation of the calcium scale crystal, a number of phosphorus-containing scale inhibitors have been proposed in the literature. However, the utilization of such types of inhibitors (e.g. trimethylene phosphonic acid (ATMP) and polyether polyaminomethylene phosphonate (PAPEMP)) could lead to the eutrophication of the water when discharged to the rivers [Ketrane et al. 2009, Zhang et al. 2017, Yang et al. 2017, Wang et al. 2016]. With the enhancement of people's awareness of environmental protection, the phosphorus-free and green inhibitor has attracted wide attention from the scientific community [Abd-El-Khalek et al. 2016]. One representative green inhibitor is polyaspartic acid (PASP). In order to further expand the comprehensive performance of scale and corrosion inhibition, grafted modification of PASP has been studied in the literature [Shi et al. 2016, Zhang et al. 2016]. By introducing new functional groups, such as carboxyl, sulfonic, and sulfhydryl, etc., new polymers can be obtained and the performance of the PASP is enhanced [Zhou et al. 2021, Shi et al. 2018]. This is because the polymers have high solubility, good fluidity, and a large number of terminated functional groups. On top of that, the polymers can be easily adsorbed on the surface of the $CaCO_3$ and $CaSO_4$ crystals. For example, Fu et al. [Fu et al. 2020] and Chen et al. [Chen et al. 2020] synthesized polyaspartic acid grafted β-cyclodextrin, and polyaspartic acid/oxidized starch copolymer (PASP/GO), respectively, which showed their good anti-scale performances to $CaSO_4$ and $CaCO_3$. Sun et al. [Sun et al. 2015] synthesized the graft copolymer of polyaspartic acid-tryptophan by introducing carboxyl and unsaturated heterocyclic groups, which improved the scale inhibition performance compared with the conventional PASP. Zhao et al. [Zhao et al. 2021] developed the graft copolymer of poly (aspartic acid) / aminomethanesulfonic acid and demonstrated its good anti-scale performance as an oilfield scale inhibitor.

In addition, the concentration of the corrosive ions (e.g. Cl^- and SO_4^{2-}) is also increased when the cooling water is recycled, which induces the corrosion products (e.g. Fe_2O_3) to attach on the pipeline and reduces the heat transfer efficiency [Farag and Hegazy 2013, Fu et al. 2010]. In order to relieve this issue, Zeino et al. [Zeino et al. 2018] proposed the PASP with Zn^{2+} as a new inhibitor, enhancing the efficiency to 97 % through a synergistic mechanism. Gao et al [Gao et al., 2015] studied a mixture of PASP-SEA-ASP, Zn^{2+}, 2-hydroxyphosphonoacetic acid (HPAA), and hexadecylldimethyl (2-sulfite) ethyl ammonium. The authors reported good corrosion inhibition performance in seawater. To further reduce the use of heavy metal ions, polyaspartic acid was modified with small green molecules containing amino groups. Chai et al [Chai et al. 2020] examined dopamine modified PASP, whose corrosion inhibition efficiency in the acid solution is relatively high because of the effective adsorption of its molecule on the metal surface. Migahed et al. [Migahed et al. 2016] synthesized polyaspartic acid/glycine graft copolymer and the corrosion inhibition efficiency of the GLY-PASP compound reached for 83.8 % at 250 mg/L. Chen et al. [Chen et al. 2019] grafted threonine onto the side chain of PASP to synthesize a polyaspartate threonine derivative (PASP-THR). From the experimental results, it was demonstrated that the inhibition efficiency of PASP-THR was greatly higher than that of PASP. As discussed above, the existing works in the literature mainly utilize the amino from amino acid to improve the inhibition performance by introducing it into the conventional PASP. Glycidyl(Gly) is mutually soluble in water and has active chemical properties. Moreover, it contains hydroxyl and ester groups and can occur esterification with a carboxylic acid. Therefore, Gly is regarded as a good modifier. For example, Huang et al. [Huang et al. 2019] studied the scale inhibition performance of polyepoxysuccinic acid modified by Gly, which is environmentally friendly and possesses high scale inhibition efficiency.

However, to the best of our knowledge, there is no report in the literature about using hydroxyl and ester from Gly to simultaneously improve the scale and the corrosion inhibition efficiency of PASP in simulated industrial water. Based on the above-mentioned findings, Gly was selected and linked to the side chain of PASP through a simple ring-opening grafting reaction of polysuccinimide (PSI) to prepare a novel PASP derivative (PASPG) in this work. Then, the comprehensive scale inhibition and the corrosion inhibition performance of PASPG were investigated by using the static scale inhibition method, weight loss method, and the electrochemical measurement method in the simulated industrial water. On these bases, in terms of the measurement of the scale inhibition mechanism, Fourier transform infrared spectroscopy(FTIR) and scanning electron microscope(SEM) experiments were also conducted to visualize the change in the morphology of both the $CaCO_3$ and $CaSO_4$ crystals. The adsorption behaviour and mechanism of PASPG on the Q235 steel surface were discussed. As expected, in comparison with PASP, PASPG, and blank showed greatly improved scale inhibition and corrosion inhibition performance due to the presence of pendent functional groups.

2. Experimental

2.1. Reagents and instruments

PSI and Gly was obtained from Shanghai Kangtuo Chemical Co. ltd. (Shanghai, P.R. China). Sodium hydroxide, anhydrous calcium chloride, anhydrous sodium sulfate, absolute ethanol, sodium bicarbonate, EDTA disodium was purchased from Tianjin Yongda Chemical Reagents Co., ltd (Tianjin, P. R. China). All reagents mentioned above are reagent grade and used without further purification. The specimen of Q235 Carbon steel ($72.4 \times 11.5 \times 2$ mm^3) were supplied by Gaoyou Qinyou Instrument Chemical Co., ltd (Gaoyou, P.R. China).

Instruments utilized in the experiments include VERTEX7O Fourier Infrared Spectroscopy (FTIR), Tga-4000 Thermogravimetric analyzer(TGA), SIGMA300 scanning electron microscopy(SEM), Pulsar TM NUCLEAR magnetic resonance spectrometer(^{1}H NMR) and Zahner Electrochemical Workstation.

2.2. Synthesis of PASP and PASPG

PASP was synthesized according to steps in paper [Chen et al. 2019].

The proposed PASPG was synthesized by PSI and Gly. First, 5 g PSI and certain amounts of Gly were added. Secondly, 1.6 g initiator sodium hydroxide and 5 mL of tetrahydrofuran solvent (THF) were added to the PSI and Gly system (the ratio was 1, 1:0.2, 1:0.4, 1:0.6, 1:0.8) and was heated to 70 °C for 6 h. After the reaction, the pH of the mixture is adjusted at 7.0 using HCl solution and then poured into certain amounts of absolute ethanol to generate precipitation. Next, the precipitation is washed by absolute ethanol and dried at 60 °C. Fig. 1 shows the synthesis reaction.

2.3. Characterization of PASPG

2.3.1. Molecular structure

In this paper, the molecular structure of PASPG was analyzed by three different methods:

(i) ^{1}H NMR. Dissolved by the heavy water (D_2O), PASPG was analyzed by PulsarTM (shanghai HaoLang Scientific Instrument Co. ltd.).

(ii) FTIR. The FTIR spectrum of PASPG was detected by VERTEX7O FTIR spectrometer (Brock Technology Co., ltd.) in the range of 4000 $\sim$ 400 cm^{-1}.

(iii) TGA. The TGA of PASPG were detected by tga-4000 thermogravimetric analyzer (PerkinElmer)in the range of 30–600 °C. Note that the heating rate was maintained at 30 °C/min in nitrogen atmosphere.

2.3.2. Molecular weight

The molecular weights of PASP and PASPG were measured by the method of Ubbelohde Viscometer. Note that the 0.8 mm Ubbelohde viscometer and sodium thiocyanate solution (105 g/L) were used. The outflow time of sodium thiocyanate solution with and without PASPG (PASP) were measured by the stop-watch and recorded as t_0 and t_1, respectively. The experiment was repeated for 3 times and the average time was used to calculate the molecular weight of PASPG (PASP), which is shown as follows:

$$\eta = KM^{\alpha} \tag{1}$$

where M is the molecular weight, K and α are the constant values ($K = 1.21 \times 10^{-3}$, $\alpha = 0.5$) [Liu et al., 2014; Huang et al., 2019] and η is calculated as (2).

$$\eta = \sqrt{2(\eta_{SP} - \ln \eta_r)}/C \tag{2}$$

where C is the concentration of PASPG (PASP)

$$\eta_{sp} = \frac{t - t_0}{t_0}\eta_r = t/t_0 \tag{3}$$

2.4. Measurement of scale inhibition efficiency

In the experiments, the scale inhibition efficiency of PASP and PASPG against $CaCO_3$ was evaluated according to the national standard (GB/T16632-2019) in China (GB/T 16632–2019). Certain amounts of anhydrous $CaCl_2$ and $NaHCO_3$ were dissolved in the deionized water and $\rho(Ca^{2+})$ = 200-mg/L and $\rho(HCO_3^-)$ = 400 mg/L[Chen et al., 2020; Liu et al., 2014; Zhou et al., 2021]. The prepared solutions with different concentrations of PASP and PASPG were heated at 60℃ for 10 h. When the solution was cooled to the room temperature, it was filtered and the concentration of Ca^{2+} was measured by the method of EDTA titration under the PH value of 12–13. Noted that the indicator was calcium carboxylic acid (the color changed from wine red to blue).

The scale inhibition efficiency can be calculated as:

$$E = \frac{A_2 - A_1}{A_0 - A_1} \times 100\% \tag{4}$$

where A_2 and A_1 are the concentration of Ca^{2+} (mg/L) in the solution with and without the scale inhibitor after heating, respectively, and A_0 is the concentration of Ca^{2+} (mg/L) without the sacle inhibitor before heating.

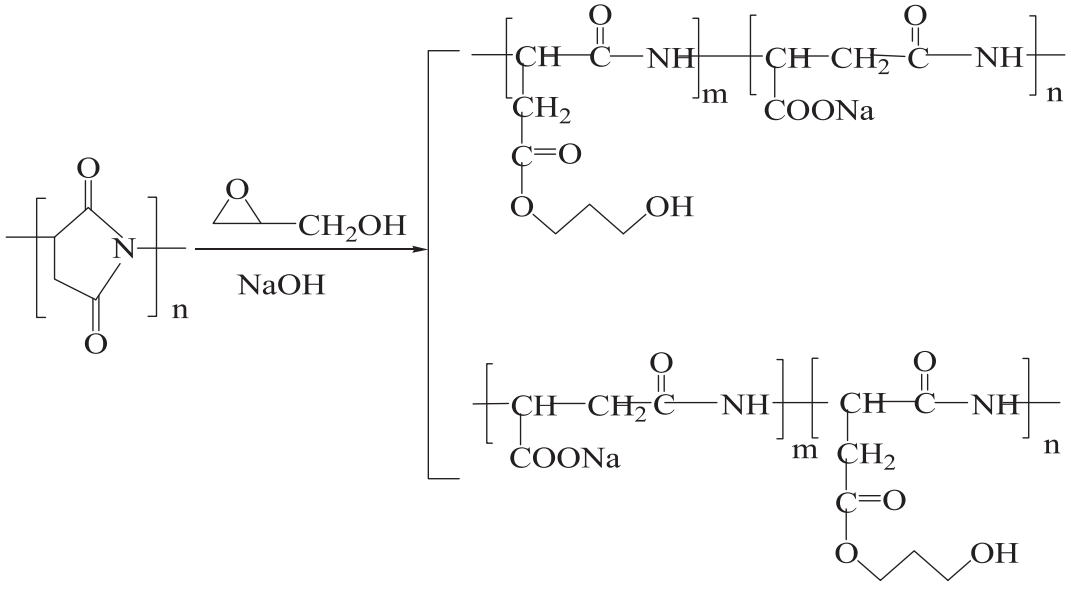

Fig. 1 Synthesis of PASP derivatives with hyper-branched by copolymerization reaction.

In terms of the scale inhibition efficiency against $CaSO_4$, all experimental conditions were identical with that of $CaCO_3$ except the concentration of $CaCl_2$ and Na_2SO_4 were 6800 mg/L and 7100 mg/L, respectively[Chen et al.2020, Zhou et al.2021].

2.5. Measurement of corrosion inhibition performance

2.5.1. Weight loss method

The to-be-tested solution was the simulated cooling water and its chemical composition was given in Table 1. The prepared carbon steel coupons (20 cm^2) was immersed in the beaker which contained 500 mL simulated cooling water and different doses of PASPG (PASP) at 25 °C. After the 3-day immersion test, the carbon steel coupons was taken out and washed by the acid (5 % HCl and 3 mg/L hexamethylenetetramine). Then, it was washed by the deionized water and dried. Finally, the carbon steel specimen was weighted with the accuracy of 0.0001 g. The testing and calculation methods were given in Chinese national standard (GB/T 18175–2014).

2.5.2. Electrochemical method

In this paper, we conducted the electrochemical experiments by Zahner electrochemical workstation with a conventional three electrode's cell. The saturated calomel electrode (SCE) was utilized as the reference electrode. In addition, platinum plate and cylindrical carbon steel (d = 2 mm) were used as counter electrode and working electrode, respectively. The to-be-tested solution was simulated cooling water containing PASPG (PASP) and the concentration was 0 and 500 mg/L. Before experiments, the working electrode was immersed in the to-be-tested solution for 30 min to obtain the steady-state open circuit potential (OCP)(Fig. 2). Note that the whole electrochemical experiments were conducted at 25 °C.

The curves of the potentiodynamic polarization were obtained from $-0.25 \sim 0.25$ V with respect to OCP at the constant scanning rate, i.e. 1 mV/s[Tan et al.2022, Tan et al.2021]. The linear parts of both anode and cathode curves were extrapolated to the corrosion potential (E_{corr}) and obtained the corrosion current density (I_{corr}), which could be utilized to calculate the corrosion inhibition efficiency of PSAPG (PASP):

$$\eta\% = \frac{i_{corr1} - i_{corr2}}{i_{corr1}} \times 100 \quad (5)$$

where i_{corr1} and i_{corr2} are the current density of the blank solution and the to-be-tested solution containing PASPG (PASP), respectively ($\mu A/cm^2$).

The electrochemical impedance spectroscopy (EIS) was obtained by utilizing the AC signals with the peak-to-peak of 5 mV at OCP and the frequency range is from 100000 Hz to 0.01 Hz[Tan et al.2022, Tan et al.2021]. The result was shown in the form of Nyquist plots. The equivalent circuit and charge transfer resistance (R_{ct}) were obtained based on Nyquist plots. Hence, the corrosion inhibition efficiency could be formulated as:

$$\eta\% = \frac{R_{ct2} - R_{ct1}}{R_{ct2}} \times 100 \quad (6)$$

where R_{ct1} and R_{ct2} are the charge transfer resistance of the blank solution and PASPG(PASP)-contained solution, respectively.

Table 1 Chemical composition of the simulated cooling water.

Ion	Ca^{2+}	Cl^-	Mg^{2+}	SO_4^{2-}	Na^+	HCO_3^-
Concentration (mg/L)	200	457	48	1920	112	120

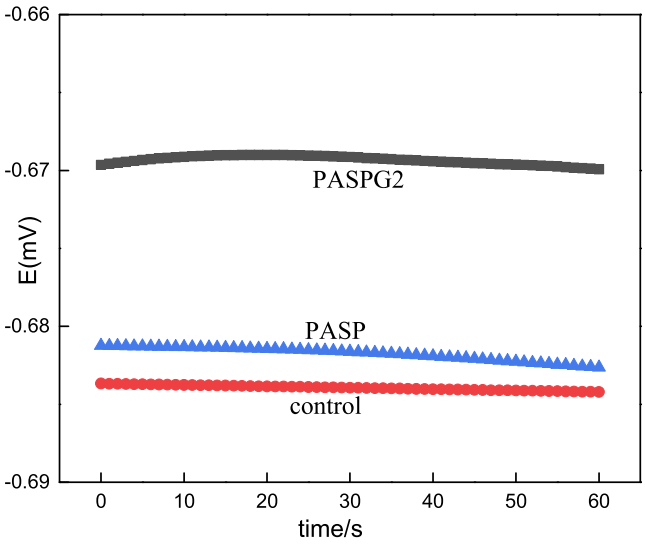

Fig. 2 E_{ocp}-t curves of Q235 steel.

2.6. SEM and EDS

In this paper, the method of obtaining $CaCO_3$ was as follows: At the room temperature, the calcium chloride, sodium bicarbonate and scale inhibitor solutions were mixed in a glass container and stirred by a magnetic stirrer. The well-mixed solution was set for 24 h. Next, $CaCO_3$ was collected by centrifugation and washed by distilled water for twice to remove the residual PASPG [Meng et al.2007, Naka 2003].

Based on the collected $CaCO_3$ crystal, SEM (SIGAM 300) was applied to obtain the final images.

On the other hand, we also visualized the protective film on the surface of the corroded carbon steel specimen by SEM. In addition, energy Dispersive Spectrometer (EDS) technology was also applied to investigate the composition of protective film.

3. Results and discussion

3.1. Analysis of the structure of PSAPG

Based on the measurement method presented in section 2.3.2, PASPG (PASP) with different molecular weights is listed in Table 2, where different mass ratios between PSI and Gly are utilized. Note that the PASPG2 in Table 2 was selected for characterization experiments of ^1H NMR and FTIR. The experimental results of ^1H NMR, FTIR, and TGA are given in Fig. 3(a), Fig. 3(b), and Fig. 3(c), respectively.

Table 2 Molecular weights of PASP and PASPG with different monomer ratios.

PSI:Gly	t_0	t_1	η_r	η_{sp}	η	M_η
1:0.0 (PASP)	120.49	125.99	1.0456	0.0456	0.0413	1162
1:0.2 (PASPG1)	120.49	126.63	1.0509	0.0509	0.0434	1286
1:0.4 (PASPG2)	120.49	127.45	1.0578	0.0578	0.0455	1414
1:0.6 (PASPG3)	120.49	128.72	1.0660	0.0660	0.0534	1948
1:0.8 (PASPG4)	120.49	129.57	1.0754	0.0754	0.0624	2661

As shown in Fig. 3(a), the peaks of 4.388 ppm and 3.502 ppm in the PASP spectrum indicate the chemical shift of the –CH- and –CONH- bonds, respectively. In addition, the peaks of 3.094 ppm and 1.547 ppm in the PASPG2 spectrum specify the chemical shift of the $–CH_2$- and $–CH_2OH$-bonds in glycidyl, respectively. Moreover, the hydrogen shift and peak of the tertiary carbon of PASPG2 have certain changes compared with that of PASP because of the graft reaction. This outcome demonstrates that glycidyl reacts with polysuccinimide and the branch point is formed.

In the PASP curve of Fig. 3(b), the absorption peaks located at 3426 cm^{-1}, 1625 cm^{-1}, and 1584 cm^{-1} indicate the stretching vibration of N—H bond, C═O of carboxyl, and C═O of amide. Besides, the absorption peak in 1404 cm^{-1} indicates the vibration of the N—H and C—N bonds of –CONH–. However, in the PASPG curve, all peaks mentioned above can be found and the peak at 2943 cm^{-1}, indicating that the vibration of $–CH_2–$ is strengthened and has a certain shift. In addition, the absorption peaks at 1047 cm^{-1} and 1196 cm^{-1}, respectively, indicate the vibration of the C—O and –OH bonds of $–CH_2$-OH. It should be mentioned that the $–CH_2$-OH group only could be found in glycidyl, which demonstrates polysuccinamide reacts with glycidyl, and PASPG2 were obtained.

In Fig. 3(c), the evaporation of the water and organic matter occurred at 30 ~ 180 °C, the rupture of the C—C covalent bond took place at 140 ~ 250 °C, the thermal degradation of –CONH- and other organic groups occurred at 250 ~ 430 °C. However, the rupture of PASPG macromolecular chain and the coking of small molecules occurred at 430 ~ 600 °C (Fu Ch.'E et al., 2011). These experimental results demonstrate that PASPG cannot be decomposed even at a relatively high temperature. For example, its mass fraction is higher than 85 % at 200 °C, which indicates its superior stability. Besides, it was also found that the curves of PASPG1 and PASPG4 contained 4 different phases from room temperature to 600 °C. However, the curves of PASPG2 and PASPG3 only

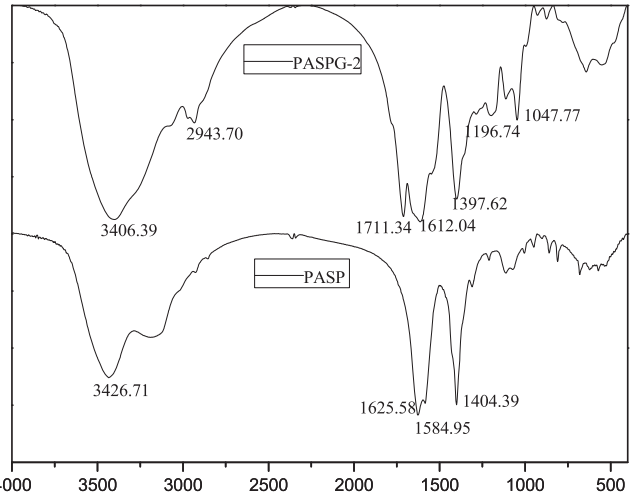

Fig. 3b The FTIR spectra of PASP and PASPG2.

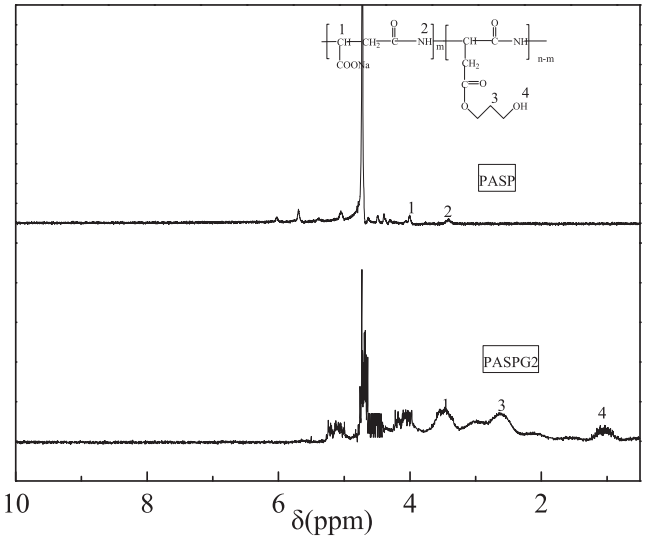

Fig. 3a The ^1H NMR spectra of PASP and PASPG2.

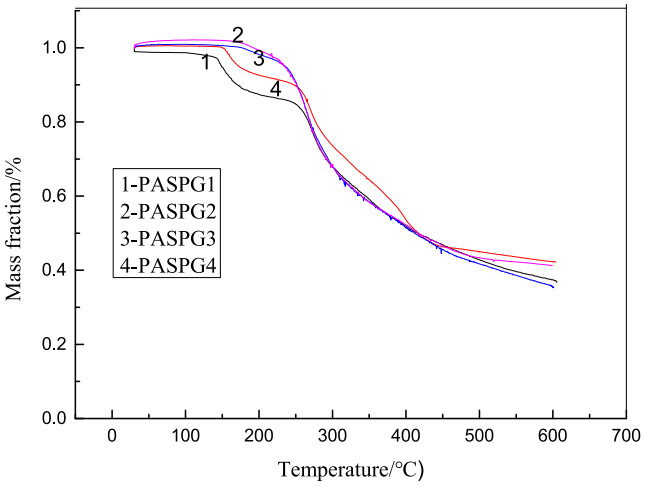

Fig. 3c Thermogravimetric analysis of PASPG.

contained 3 different phases, which indicates that the stability of the latter two products was better.

3.2. Analysis of scale inhibition performance

In this section, four different factors that effect scale inhibition performance were thoroughly investigated. More specifically, they are the monomer ratio, PASPG concentration, pH value, and the concentration of Ca^{2+}.

3.2.1. Influence of monomer ratio and PASPG concentration on scale inhibition efficiency

In Fig. 4, the impact of the monomer ratio (PSI vs Gly) and the concentration of PAPSG on the scale inhibition efficiency was examined. As shown in Figs. 4(a) and 4(b), the scale inhibition efficiency of PASPG were greatly higher than that of PASP over the whole concentration range. The scale inhibition efficiency of PASPG increased first and then decreased with the change of the mass ratio of monomer. When PSI:Gly = 1:0.4(PASPG2), the scale inhibition efficiency reached the maximum. Furthermore, the scale inhibition efficiency increased as the concentration raised. However, the growth rate became slow when the concentration was higher than 25 mg/L. The scale inhibition efficiency of PASPG achieved 94.6 % and 95.1 % for $CaCO_3$ and $CaSO_4$ at the concentration of 25 mg/L, respectively. This is because the chelation effect of PASPG's branched structure on Ca^{2+} was stronger than that of PASP's linear structure [Zhang et al. 2016]. (This was also verified by the difference in the molecular weight of the aforementioned product). Besides, the lone pair electrons of oxygen ether in bonds and hydroxyls from PASPG maybe induce the adsorption of inhibitor molecules on the surface of the crystal of $CaCO_3$ and $CaSO_4$ [Huang et al. 2019].

3.2.2. Influence of pH value on $CaCO_3$ scale inhibition efficiency

In this subsection, the influence of the pH value on $CaCO_3$ scale inhibition efficiency was investigated and the results are given in Fig. 5. As can be observed, the scale inhibition performance of PASPG was stable in the whole pH range. On the contrary, the performance of PASP decreased significantly as

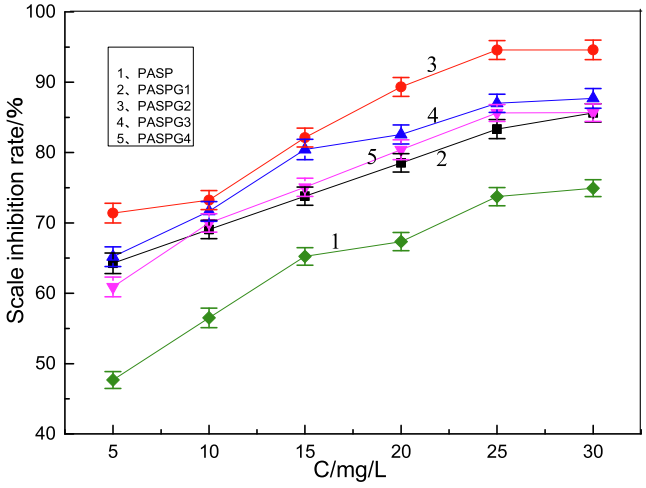

Fig. 4a Influence of mass ratios of (PSI vs Gly.) on the $CaCO_3$ scale inhibition performance.

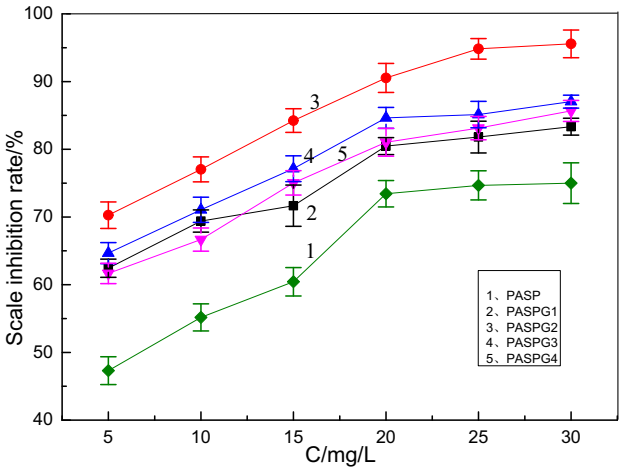

Fig. 4b Influence of mass ratios of (PSI vs Gly.) on the $CaSO_4$ scale inhibition performance.

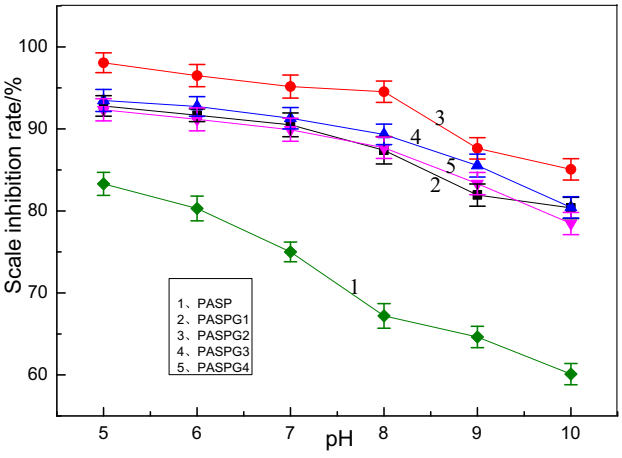

Fig. 5 The relationship between pH value and $CaCO_3$ scale inhibition performance.

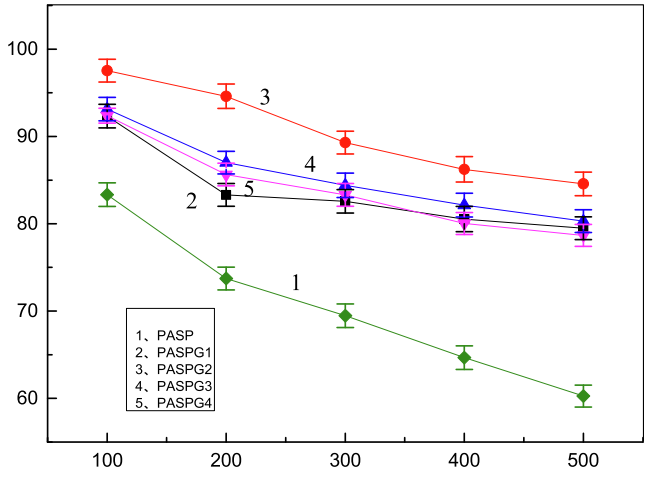

Fig. 6 The Relationship between the concentration of Ca^{2+} and $CaCO_3$ scale inhibition efficiency.

the pH value increased. The scale inhibition efficiency of PASPG2 for calcium carbonate was always higher than that of other modified products PASPG under different pH conditions. Additionally, the scale inhibition efficiency of PASPG2 was up to 85.0 %, while that of PASP was 60.1 % at pH = 10. This phenomenon can be accounted for by the chelation effect of PASPG's ether bonds and hydroxyls, which was stronger than that of PASP's carboxyl group. However, the chelation effect of PASPG on Ca^{2+} maybe be weakened by the alkaline environment, resulting in a slight performance loss when the pH value was higher than 8 [Bukuaghangin et al. 2016]. Therefore, it can be concluded that a pH value of 5 ~ 9 is the best condition for PASPG to be used as a $CaCO_3$ scale inhibitor.

3.2.3. Influence of the concentration of Ca^{2+} on $CaCO_3$ scale inhibition efficiency

Fig. 6 depicts the experimental results of the relationship between the concentration of Ca^{2+} and the $CaCO_3$ scale inhibition efficiency, where the concentration of PASPG (PASP) was 25 mg/L. As can be ascertained from Fig. 6, compared with PASP, the proposed PASPG's performance reduced slowly as the concentration of Ca^{2+} increased. In different concentration values of Ca^{2+} systems, the scale inhibition efficiency of PASPG with different monomer mass ratios was obviously higher than that of PASP. When [Ca^{2+}] = 500-mg/L, the scale inhibition efficiency of PASPG2 was up to 84.6 %, while that of PASP was 60.3 %.

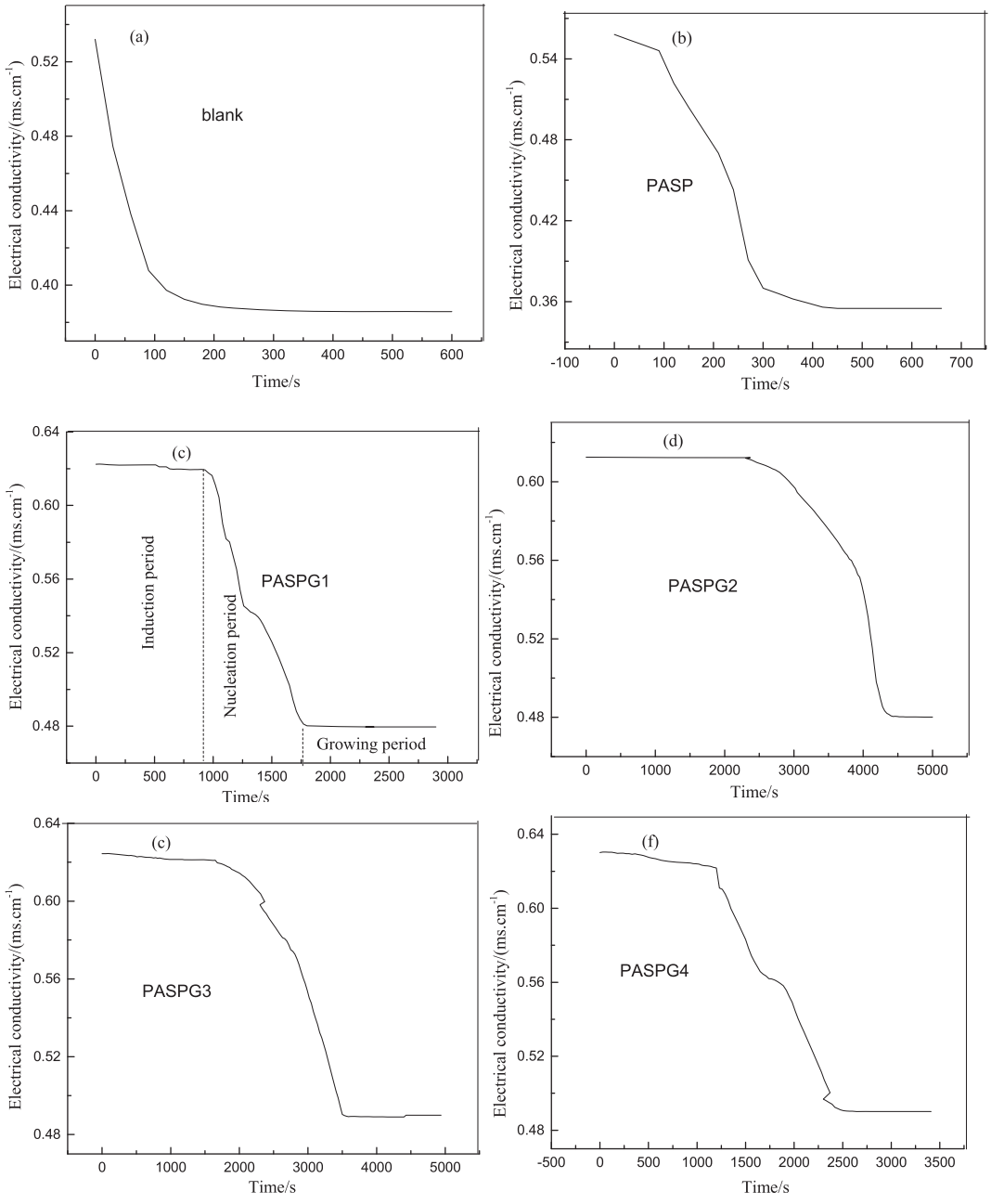

Fig. 7 The electric conductivity of solution with different inhibitors (a. Blank, b. PASP, c. PASPG1, d. PASPG2, e. PASPG3, f. PASPG4).

This phenomenon indicates that the scale inhibition efficiency of PASPG was robust with the concentration of Ca^{2+}.

3.3. Scale inhibition mechanism

In this section, the scale inhibition mechanism was investigated from three aspects: the nucleation process of the calcium crystal, FTIR spectrum, and SEM images.

3.3.1. Nucleation process of $CaCO_3$ crystal

In this subsection, the nucleation process of $CaCO_3$ crystal was indicated by a change of the electrical conductivity with a conductivity meter (SLDS-1, made in Nanjing Sangli Electronic Equipment Factory in China). Fig. 7 shows that the change in the electrical conductivity of the mixed solution (264 mg/L calcium chloride, 252 mg/L sodium carbonate, and 20 mg/L scale inhibitor) versus the time when the different inhibitors were utilized. More specifically, as shown in Fig. 7(a), the electrical conductivity of the blank group without the inhibitor significantly decreased, which indicates the absence of a nucleation induction period. However, the nucleation induction period of $CaCO_3$ in PASPG groups ranged from 900 s to 2300 s (Fig. 7(c)-7(e)). On the contrary, the period in the PASP group was about 100 s (Fig. 7(b)), which demonstrates that the proposed PASPG's hyperbranched structure can effectively prolong the nucleation induction period of the $CaCO_3$. In addition, the PASPG2 (Fig. 7(d)) showed the best inhibition performance.

Furthermore, when the reaction achieved the state of equilibrium, the concentration of Ca^{2+} in the PASPG groups was higher than that of the control group and the PASP group, which demonstrates that PASPG improves the solubility of the $CaCO_3$ crystal in the solution. This phenomenon can be explained by formula (7) [Huang et al. 2019]:

$$\ln\frac{c}{c_0} = \frac{2\gamma M}{RT\rho r_c} \tag{7}$$

where c and c_0 represent the concentrations of $CaCO_3$ in the solution with and without inhibitor respectively, γ, M, and ρ, denote the surface energy, molar mass, and density of $CaCO_3$ crystal, respectively. R is a constant and equal to 8.314, T refers to the temperature, and r_c denotes the critical radius of the crystal.

According to formula (7), when the concentration of $CaCO_3$ increases, the critical radius of the $CaCO_3$ crystal will be smaller. Therefore, it can be argued that PASPG is more effective for scale inhibition compared with PASP.

3.3.2. FTIR analysis of $CaCO_3$ crystal

The polymorphs of $CaCO_3$ crystal are different when the utilized inhibitor is different. The FTIR spectrum of the $CaCO_3$ crystal is given in Fig. 8 (Fig. 8b shows a partial enlargement of Fig. 8a), where the adsorption peaks at 711 cm^{-1} and 745 cm^{-1} represent the calcite and the vaterite polymorphs of $CaCO_3$ crystal, respectively [Meng,wt al. 2007. Naka 2003]. As shown obviously in Fig. 8b, only calcite was found in the blank group and both the alcite and the vaterite exist in the PASP and PASPG groups. This is because the inhibitor occupied the distorted position of vaterite with double inverted cones in some cases and the calcite was not formed [Zhang et al. 2017].

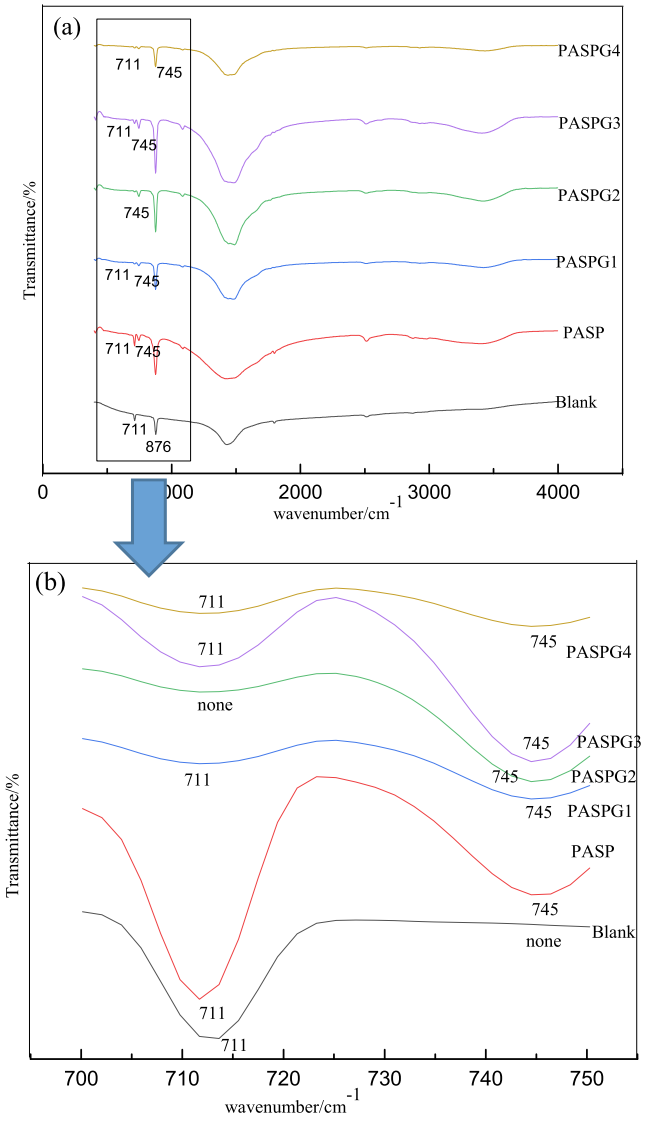

Fig. 8 FTIR spectra of $CaCO_3$ crystal with different inhibitors.

More specifically, compared with the PASP group, most of the polymorphs of $CaCO_3$ crystal in the PASPG2 were vaterite, which corresponds to the curve of PASPG2 (there is no obvious adsorption peak at 711 cm^{-1}). This phenomenon can be accounted for by the fact that PASPG2′s adsorption capacity on $CaCO_3$ crystal was significantly stronger than that of PASP.

3.3.3. Morphology of calcium crystal

a) SEM analysis of $CaCO_3$.

The $CaCO_3$ crystal was prepared by using different inhibitors with a concentration of 25 mg/L. whereas the SEM images of the $CaCO_3$ crystal are shown in Fig. 9. From Fig. 9 (a), it can be seen that the crystal in the blank group possesses a smooth surface and hard texture. Although the lattice distortion occurred both in the PSAP and PSAPG groups, the size of the crystal in the PASPG groups obviously appeared to be smaller. In addition, the crystal in the PASPG2 group was the loosest. By comparing the morphology of calcium carbonate of the control group with that of the added scale inhi-

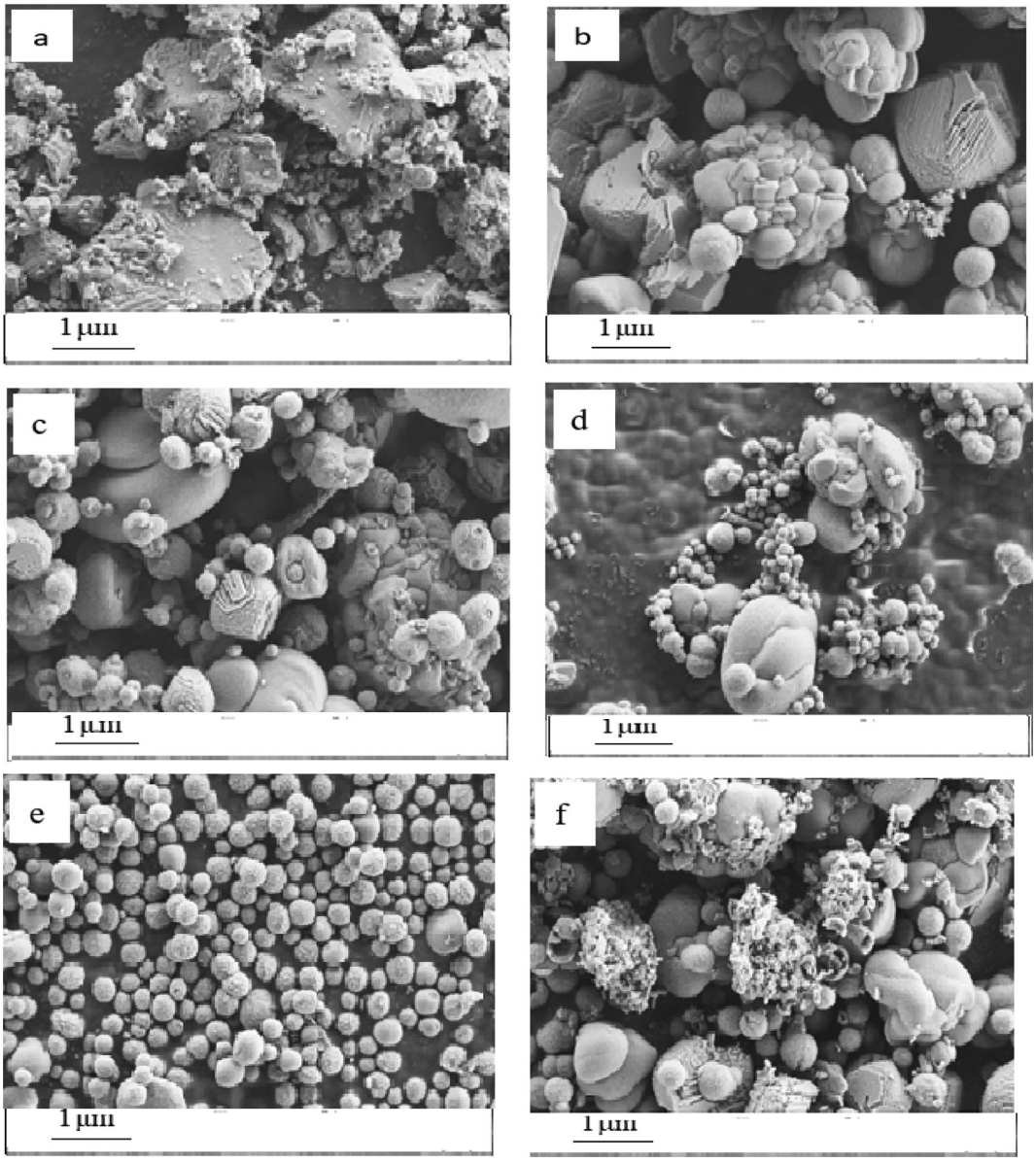

Fig. 9 SEM images of $CaCO_3$ with different inhibitors [(a) blank, (b) PASP, (c) PASPG1, (d) PASPG2, (e) PASPG3, (f) PASPG4].

bitor, it was proved that the crystalline form of calcium carbonate was from calcite to vaterite [Chen et al. 2015, Huang et al. 2019, Ge et al. 2016, Nan et al. 2010].

In order to clearly explain the morphology changes of the $CaCO_3$ crystal, a schematic diagram was provided in Fig. 10. As can be observed, the top half represents the change of the shape of the crystal without the inhibitor and the calcite was formed at last. When the PASPG (PASP) was formed, the lattice distortion occurred and the formation of calcite was inhibited, as shown in the bottom half of Fig. 10.

b) SEM analysis of $CaSO_4$.

The SEM images of $CaSO_4$ are shown in Fig. 11. Particularly, from Fig. 11(a), it can be seen that the crystal is regular and smooth in the blank group. Additionally, when the conventional PASP (25 mg/L) was added, fine cracks can be found on the surface of the crystal from Fig. 11 (b). However, as shown in Fig. 11(c)-11(f) (the 25 mg/L PASPG was added), the crystal were deepened and its surface appeared to be rougher and full of honeycombs. Besides, the whisker of the crystal disappeared and also the length-diameter ratio decreased significantly. More concretely, the crystal of $CaSO_4$ was broken completely into small and unstable crystals when PASPG2 was added. This was because the branched polymer molecules were adsorbed on the surface of the microcrystal and inhibited the growth of the $CaSO_4$ crystal [Huang et al. 2019]. In this case, the scale was prevented from sticking to the pipeline and can be easily washed away by the running water.

3.4. Analysis of the corrosion inhibition performance

In this section, the weight loss method, electrochemical method, SEM technology, and EDS technology were applied to evaluate the corrosion inhibition performance of PASPG (PASP).

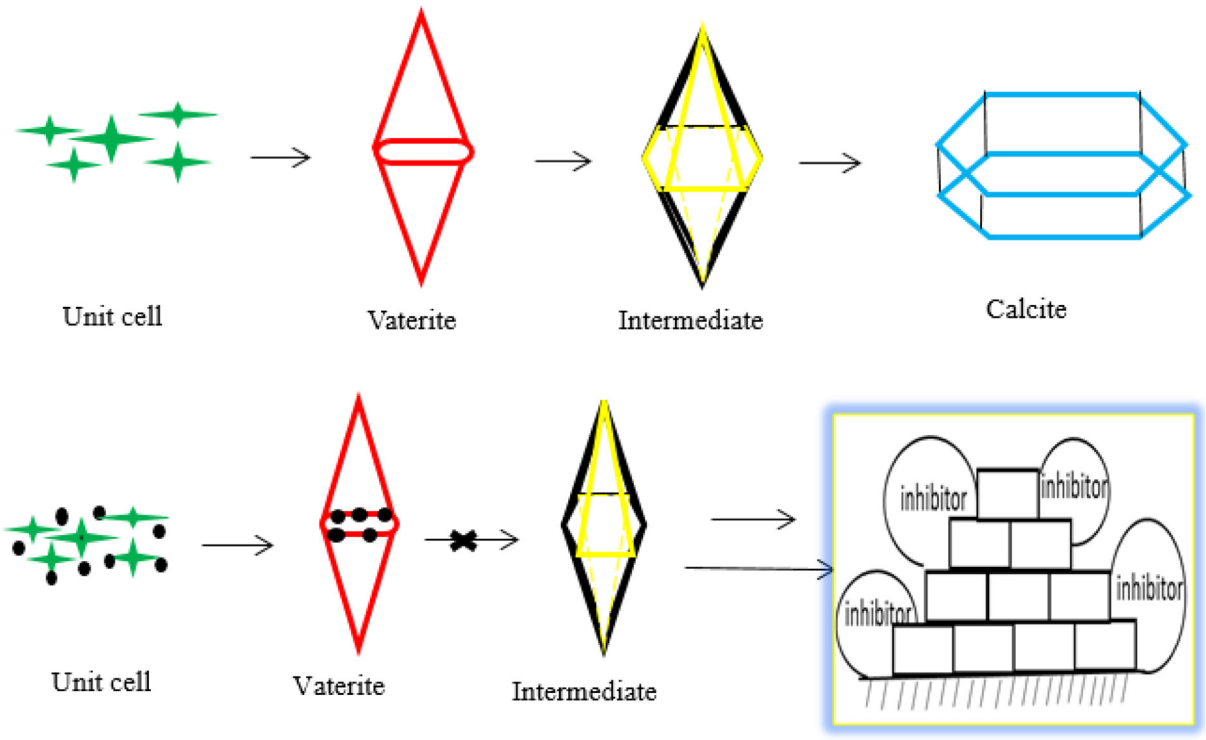

Fig. 10 The change of morphology of $CaCO_3$ crystal with and without inhibitor.

3.4.1. Weight loss test

In this subsection, the weight loss method was utilized to measure the corrosion inhibition efficiency of PASP and PASPG for 72 h at the temperature value of 25 °C [Chen et al. 2019]. The experimental results are given in Table 3, where only PASPG2 was considered as the representation of the PASPG inhibitor. As presented in Table 3, the corrosion efficiency increased when the concentration of PASPG2 (PASP) became higher. Besides, it can be seen that the corrosion efficiency of PASPG2 was higher than that of PASP with an identical concentration. As an example, the efficiency of PASPG2 at 500 mg/L was 85.17 %, while it was 72.53 % for PASP. This is because more area of the steel surface was covered and the influence of the chemical adsorption was strengthened when PASPG2 is compared with PASP.

3.4.2. Electrochemical test

In this subsection, two classical electrochemical experiments, namely the polarization test and impedance test were conducted to evaluate the corrosion inhibition performance of the proposed PASPG. Finally, PASPG was also compared with other inhibitors and the results in detail were analysed.

The three polarization curves in Fig. 12 are the polarization curves of blank, PASP of 500 mg/L, PASPG2 of 500 mg/L, and carbon steel of Q235 in solution, respectively. On top of that, in the original pictures, sometimes, a small tail appeared at the high potential extremity of the polarization curve plot, which can be assigned to metal dissolution. Thus, the small tails were neglected because they do not affect graphic analysis [Chen et al. 2019]. As can be seen from Fig. 12, after the addition of PASP and PASPG2, the corrosion potential (E_{coor}) had a positive shift of 10 mV and 41 Mv, respectively, compared with the blank solution, which was much less than 85 Mv [Mourya et al. 2014] (as can be seen from Table 4). Moreover, the corrosion current of the cathode and anode decreased obviously, and β_a and β_c increased to a certain extent, and the slope of the cathode curve changed greater, which proved that PASP and PASPG2 were mixed corrosion inhibitors mainly for inhibiting cathodes. The current density of PASP and PASPG2 decreased also from 15.90 μA/cm^2 to 3.71 μA/cm^2 and 2.80 μA/cm^2, respectively. What's more, the inhibition efficiency of PASP and PASPG2 was 76.67 % and 82.38 %, respectively. The inhibition efficiency of PASPG2 was also 6.61 % higher than that of PASP. Fig. 12 and Table 4 show that PASPG2 can effectively inhibit the corrosion of steel after adsorption on the interface of the Q235 steel. This further proves that PASPG2 has both good scale inhibition and corrosion inhibition performance.

The three curves in Fig. 13 are the EIS diagram of blank, PASP of 500 mg/L, and PASPG2 of 500 mg/L of Q235 carbon steel in solution, respectively. Fig. 13 illustrates that the blank, PASP, and PASPG2 systems all have an irregular semi-arc, which may be due to the roughness of the solid electrode surface and the frequency dispersion [Qiang et al. 2021, Solomon et al. 2019]. Charge transfer of impedance arc (Rct) with PASP or PASPG2 system was also greater than that of the blank, whereas, Rct of the PASPG2 was larger and the inhibition efficiency of PASPG2 was 82.35 %, which proved that PASPG2 can well inhibit the corrosion of Q235 steel in the solution.

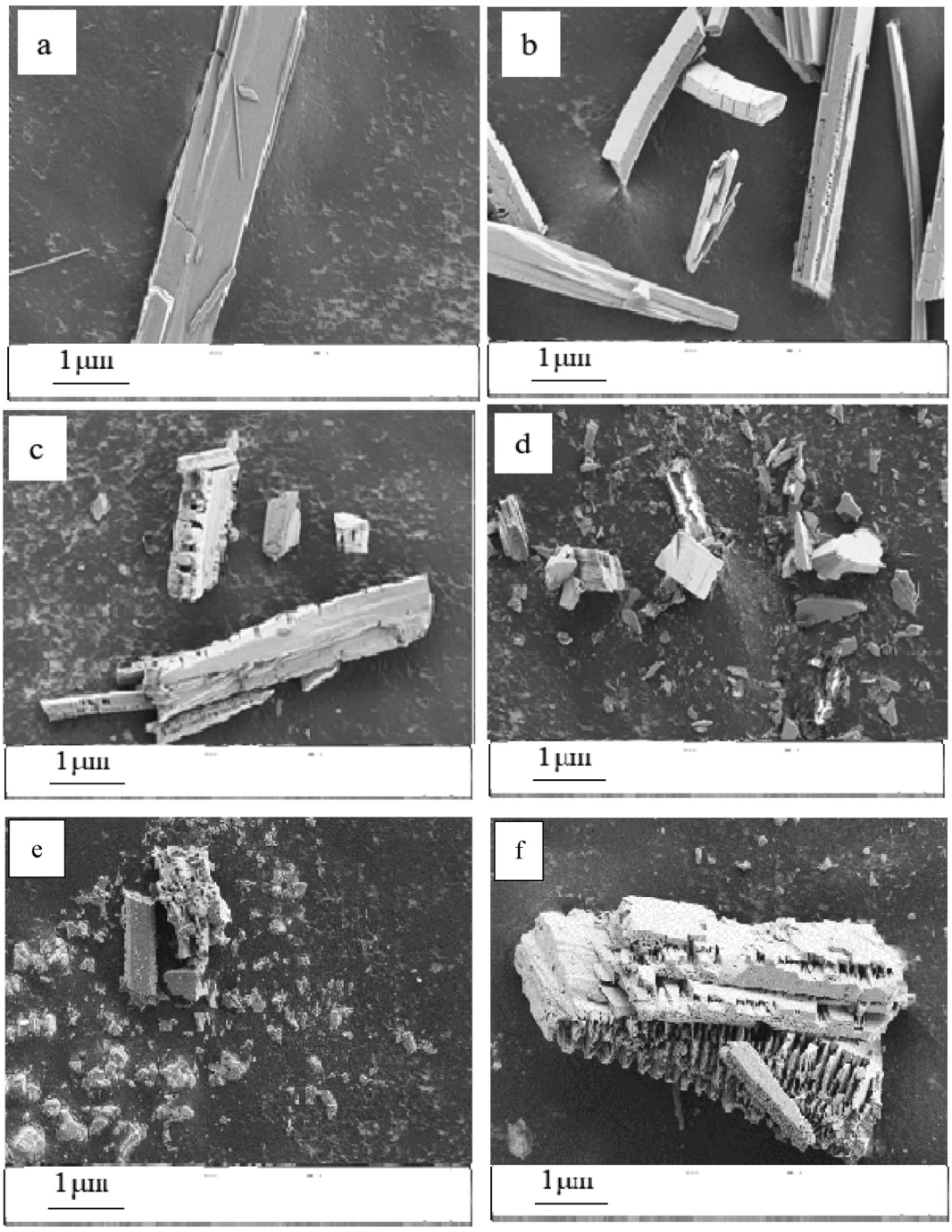

Fig. 11 SEM images of $CaSO_4$ crystal with different inhibitors (a) blank, (b) PASP, (c) PASPG1, (d) PASPG2, (e) PASPG3, (f) PASPG4.

In order to deeply understand the corrosion inhibition mechanism of PASP and PASPG2, impedance diagrams of blank, PASP, and PASPG2 systems were fitted to obtain an appropriate equivalent circuit diagram in Fig. 14 (it can be seen from Table 5 that Chi-square χ^2 represents the fitting accuracy of the data, while a low value of χ^2 indicates that the fitting results are in good agreement with the acquired experimental data) [Wan et al. 2022, Zeng et al. 2022]. In the model of the circuit diagram, R_s represents the solution resistance, R_f denotes the membrane resistance, C_f is the membrane capacitance, Y_0 refers to a constant of the constant phase element of double electrical layer capacitance(CPE), and n is the CPE index, representing the un-smoothness of the electrode surface. Because the blank, PASP, and PASPG2 systems all produce an irregular semi-arc, the ideal capacitors contained in the three systems were replaced by constant phase angles (CPE). [Replace capacitance with constant phase angle (CPE).] The calculation formula of the CPE impedance is shown in formula (8) [Qiang et al. 2021, Solomon et al. 2019]:

Table 3 Comparison of the corrosion inhibition efficiency of PASP and PASPG2.

Inhibitor	Concentration (mg/L)	X (g/cm^2.h)	η (%)
Blank	0	2.88×10^{-5}	/
PASP	50	1.93×10^{-5}	32.97
	100	1.68×10^{-5}	41.66
	150	1.375×10^{-5}	52.26
	200	1.34×10^{-5}	53.47
	300	1.07×10^{-5}	62.84
	500	7.91×10^{-6}	72.53
PASPG2	50	1.76×10^{-5}	39.06
	100	1.26×10^{-5}	56.25
	150	1.11×10^{-5}	61.45
	200	1.01×10^{-5}	64.93
	300	7.42×10^{-6}	74.25
	500	4.27×10^{-6}	85.17

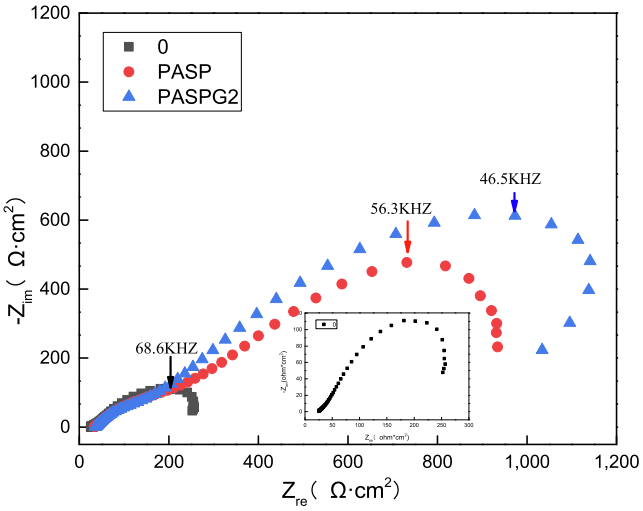

Fig. 13 Nyquist plots of blank, PASP, and PASPG2.

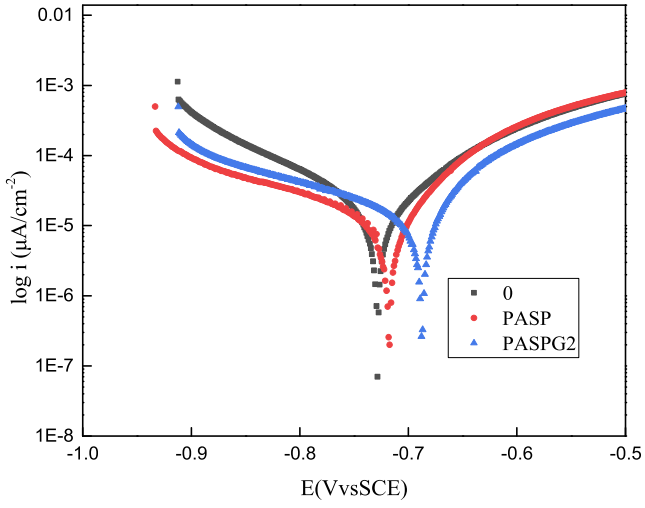

Fig. 12 Tafel polarization curves of blank, PASP, and PASPG2.

Table 4 Polarization parameters of the carbon steel without and with PASP or PASPG2.

Inhibitor	E_{corr} (mVvs SCE)	I_{corr}(μA/cm^2)	βa (mV/dec)	-β_C (mV/dec)	η(%)
blank	−728	15.90	531	1.45	/
PASP	−718	3.71	255	1.01	76.67
PASPG2	−687	2.80	241	5.71	82.38

$$Z_{CPE} = \frac{1}{Y_0(j\omega)^n} \tag{8}$$

where Y_0 is the CPE constant, j denotes the imaginary root, and ω is the angular frequency.

The value of CPE_{dl} was calculated by using the formula (9) [Tan et al. 2020, Tan et al. 2022, Qiang et al. 2020]:

$$CPE_{dl} = Y_0(\omega)^{n-1} = Y_0(2\pi f_{Zim-\max})^{n-1} \tag{9}$$

As can be observed from Table 5, the value of CPE_{dl} was reduced in the PASP and PASPG2 system in comparison with

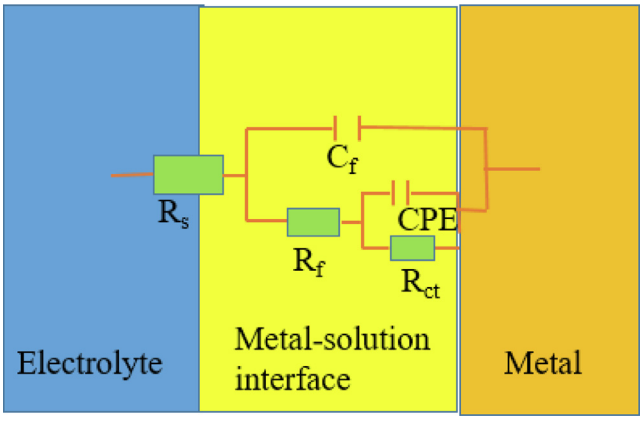

Fig. 14 The equivalent circuit for fitting the impedance spectra of the carbon steel.

that of the blank system, whereas the PASPG2 system was smaller. By using the following formula (10) [Dehghani et al. 2019, Wan et al. 2022]:

$$CPE_{dl} = \frac{\varepsilon^0 \varepsilon}{d} S \tag{10}$$

where ε^0 and ε represent the dielectric constant of air and the local dielectric constant of the double electric layer, respectively. S stands for the electrode area of Q235 steel, and d denotes the thickness of the double-layer capacitor. A denser layer of adsorption protective film was also formed on the surface of the Q235 steel/solution as the PASP and PASPG2 molecules replace H_2O molecules on the surface of Q235 steel, and the PASPG2 molecules contained more adsorption centers, making it easier for PASPG2 to be adsorbed on the surface of the carbon steel. In addition, CPE_{dl} was smaller because (i) the dielectric constant of the PASPG2 molecule was smaller than that of the water molecule, whereas PASPG2 after adsorption can effectively reduce the value of the local dielectric constant (ε). (ii) the molecular volume of PASPG2 was significantly larger than those of H_2O. Therefore, the PASPG2 adsorption on the Q235 steel/solution surface results

Table 5 Impedance Parameters of Carbon Steel Without and with PASP or PASPG2.

Inhibitor	R_S ($\Omega \cdot cm^2$)	R_f ($\Omega \cdot cm^2$)	C_f ($\mu F \cdot cm^{-2}$)	R_{ct} ($\Omega \cdot cm^2$)	CPE_{dl}		Η(%)	χ^2
					Y_0 ($10^{-4} \cdot \Omega \cdot cm^{-2} \cdot s^n$)	n		
Blank	25.8	26.3	62.4	320.3	25.0	0.762	/	0.0054
PASP	33.9	351.7	13.9	1224.6	14.0	0.751	73.84	0.0078
PASPG	35.8	247.7	10.5	1814.9	8.60	0.701	82.35	0.0040

Table 6 The Comparison of PASPG2 with other inhibitors reported in the literature.

Inhibitor	Metal exposed	Corrosive media	C_{inh}	η (%)	Reference
PASPG2	Q235 carbon steel	Simulated cooling water	300 mg/L	85.17	proposed
SA	API X60 steel	3.5 % NaCl	300 mg/L	57.57	[Obota etal.2017]
HEC	1018C-steel	3.5 % NaCl	0.1 mM	88.7	[EL-Haddad et al.2014]
PGP	Mild Steel	3.5 % NaCl	900 mg/L	64.62	[Geethanjali et al.2014]
PGP	Mild Steel	3.5 % NaCl	500 mg/L	69.57	[Geethanjali et al.2014]
PASP/SB	Q235 carbon steel	1 M HCl	80 ppm	90.39	[Wang et al.2019]
ASLE	Q235 carbon steel	1 M HCl	150 mg/L	98.79	[Liao et al.2023]

in a larger thickness of the double electric layer. The dispersion index n did not change much, indicating that the corrosion reaction of the PASPG2 reagent system was controlled by the electrochemical reaction, and the reaction process remained unchanged [Mourya et al. 2014, Qiang et al. 2021, Solomon et al. 2019, Tan et al. 2020, Qiang et al. 2020, Dehghani et al. 2019].

Besides, the corrosion inhibition efficiency among PASPG2, SA, HE, C, and PGP were also compared in Table 6 and the proposed PASPG2 achieved the best performance.

3.4.3. SEM and EDS analysis of the carbon steel specimens

In order to clearly examine the morphology of the specimen surface after corroding, SEM imaging was used for studying the morphology of the samples. In addition, EDS mapping was also applied to investigate the composition of the protective film on the surface of the specimen. The concentration of inhibitor was 500 mg/L and the experimental results are displayed in Fig. 15. As shown in Fig. 15(a), the surface of the steel in the blank group was full of corrosion products after being exposed for 72 h at the temperature value of 25 °C, which were scale and iron oxide (Fe $(OH)_3$ and FeOOH) [Chen et al. 2019]. Compared with the PASP group in Fig. 15(c), the surface of the steel in the PASPG group (Fig. 15 (e)) obviously appeared to be smoother and less corrosion product was formed. This phenomenon can also be proved by the EDS results. Compared with the PASP group in Fig. 15 (d), the oxygen content decreased and the iron atoms of the PASPG group increased significantly, as shown in Fig. 15 (f). The EDS experimental data with PASPG2 are also very close to the experimental data of the newly polished carbon steel specimen. This is because PASPG2 can be adsorbed on the steel surface and the corrosion rate became slower [Chen et al. 2019].

3.5. Mechanism of corrosion inhibition

In order to investigate the underlying mechanism of corrosion inhibition of PASG, the adsorption isotherm, and PZC tests were adopted. In addition, the whole process of corrosion inhibition is also shown in detail.

3.5.1. Adsorption isotherm

The corrosion inhibition performance of the organic inhibitor is determined by its adsorption effect on the surface of the metal. Therefore, to elaborate on the mechanism of corrosion inhibition, utilizing an adsorption isotherm formulation, such as Langmuir, Floy-Huggin, Bockris-Swinkels, Frumkin, and Temkin isotherms is an effective method [Wang et al. 2019]. More specifically, the Langmuir formula was selected in our experiments due to its best-fitting effect. Therefore, other isotherms were not taken into account.

$$\frac{C_{inh}}{\theta} = \frac{1}{K_{ads}} + C_{inh} \tag{11}$$

where C_{inh} represents the concentration of PASPG2, K_{ads} denotes the equilibrium constant of the adsorption process and θ is the surface coverage of the PASPG2 molecule on the steel surface, which is equal to the value of the corrosion inhibition efficiency obtained from the weight loss method. Note that the adsorption effect of PASPG2 molecules was positively correlated with the constant K_{ads}.

According to formula (11), the relationship between C_{inh}/θ and C_{inh} is depicted in Fig. 16 and the discrete point is fitted into a line, where the correlation coefficient is $R^2 = 0.99332$. This result indicates the adsorption behaviour of PASPG2 molecules was consistent with the Langmuir formula. It should be also mentioned that the reciprocal of the intercept of the line is the constant K_{ads}, which can be further utilized to calculate the adsorption-free energy ΔG^0_{ads}:

$$\Delta G^0_{ads} = -RTln(1 \times 10^6 K_{ads}) \tag{12}$$

where R is the standard gas constant, T refers to the thermodynamic temperature, and the constant 1×10^6 stands for the concentration of the water molecules (mg/L). The results for calculating K_{ads} and ΔG^0_{ads} are 1.1585 L/mg and −34.593 kJ/mol, respectively.

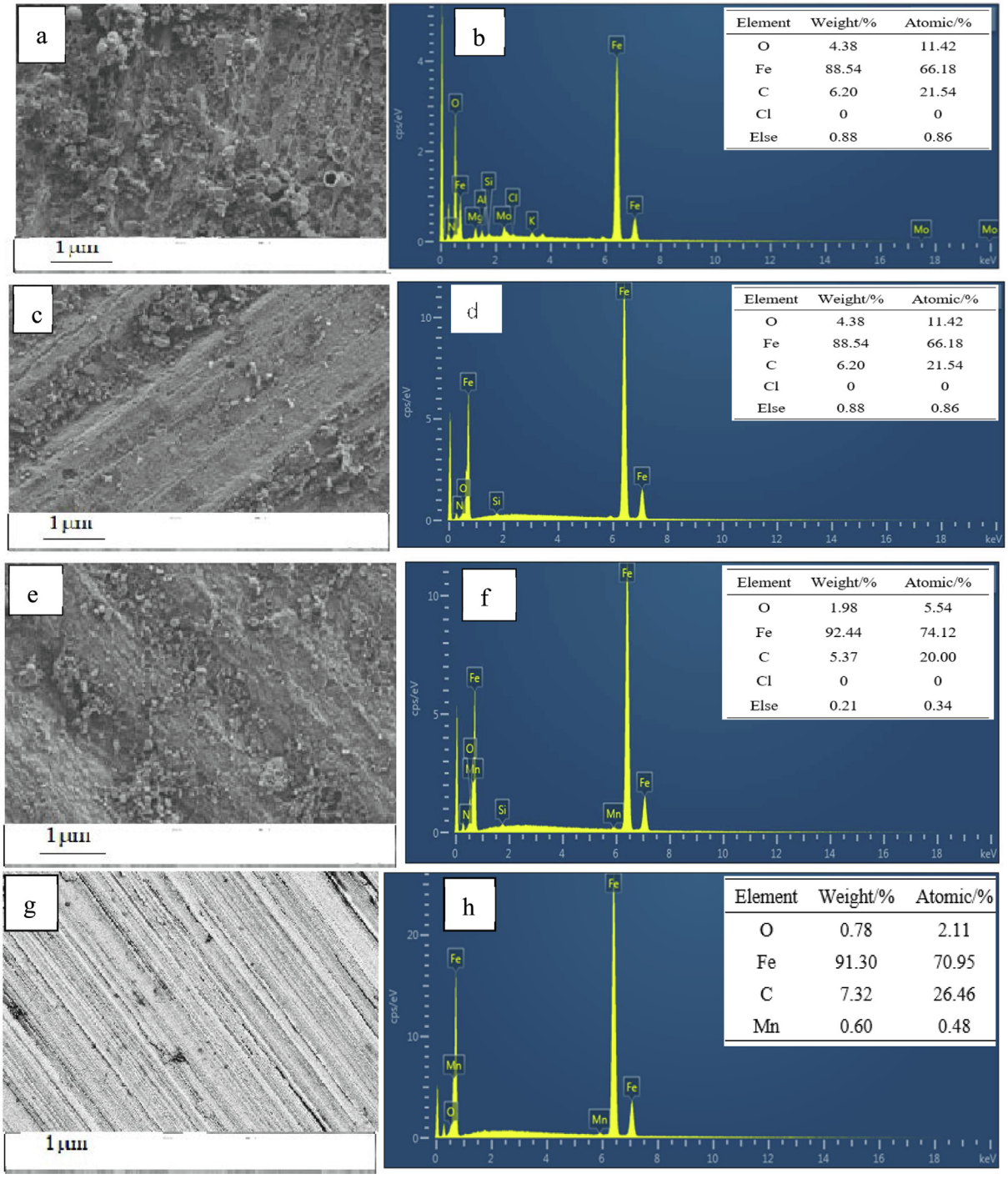

Fig. 15 SEM and EDS analyses of the carbon steel specimens. (a-b) blank, (c-d) PASP (e-f), PASPG2 (g-h) new.

When $|\Delta G^0| \leq 20$ kJ/mol, the adsorption behaviour can be considered physical adsorption because of the electrostatic interaction between the charged metal surface and the corrosion inhibitor molecules. On the other hand, chemical adsorption takes place when $|\Delta G^0| \geq 40$ kJ/mol. More concretely, it was involved in the processes of (i) the transfer and sharing of electrons and (ii) the formation of complexation covalent bonds from inhibitor molecules to the metal surface.

Based on the above-mentioned discussion, it can be concluded that the adsorption behavior of PASPG2 on the steel surface includes both physical and chemical adsorption. More specifically, in terms of physical adsorption, electrostatic attraction exists when PASPG2 molecules approach the surface of the carbon steel. Besides, the complexation behaviour between inhibitor molecules and the vacant d-orbital of the iron atom demonstrates the existence of chemical adsorption.

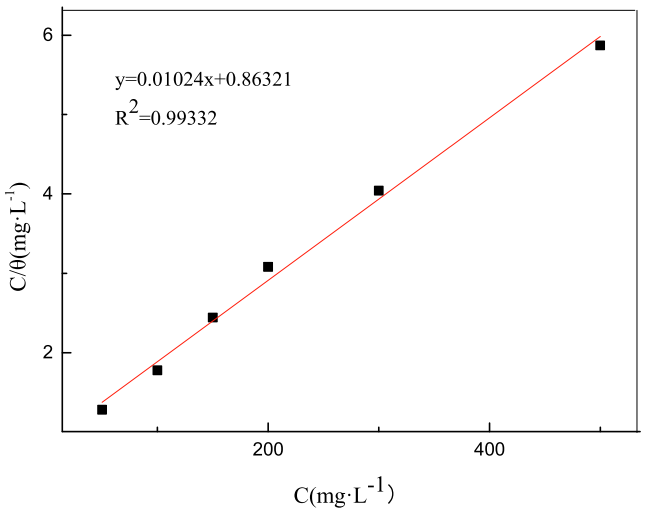

Fig. 16 Langmuir plot for the adsorption of PASPG2 on the carbon steel surface.

3.5.2. Potential of zero charge (PZC) tests

In order to clearly understand the underlying reason for the adsorption of PASAG2 molecules on the surface of the carbon steel specimen, the PZC was measured by the AC impedance method at the temperature value of 25 °C. The relationship between the double-layer capacitance (C_{dl}) and the voltage (E) is illustrated in Fig. 17, where the horizontal coordinate value of the lowest point of the parabola was PZC ($E_{pzc\ (PASPG2)}$ = -0.60 V). Therefore, the difference between PZC and the corresponding open circuit potential ($E_{ocp(PASPG2)}$ = -0.52 V) was 0.08 V (φ_{PASPG2} = 0.60–0.52 = 0.08 V). Hence, it can be concluded that first since φ_{PASPG2} was positive, the anions in the solution such as cl- and SO_4^{2-} were adsorbed on the steel surface, which will be negatively charged. Then, the anions on the steel surface became the electrostatic bond with the positively charged PAPSG2 ions [Amin et al. 2011].

3.5.3. Process of corrosion inhibition

The reaction equations of the process of corrosion inhibition are shown as follows: [Chen et al. 2019]:

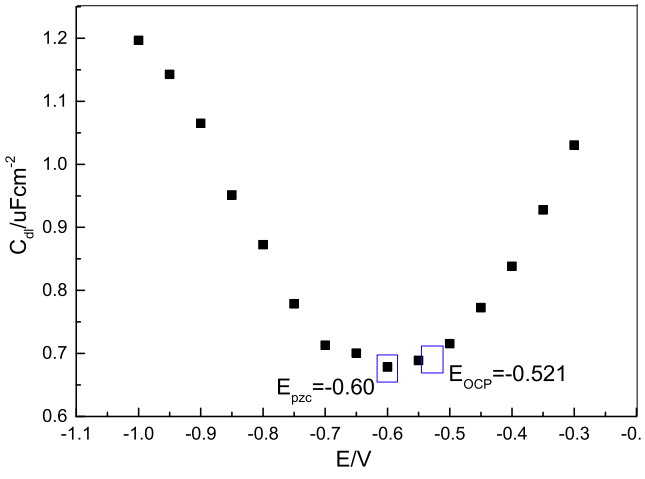

Fig. 17 The relationship between the double-layer capacitance (C_{dl}) and the voltage (E).

$$Fe \rightarrow Fe^{2+} + 2e^{-} \quad (13)$$

$$O_2 + 2H_2O + 4e^{-} \rightarrow 4OH^{-} \quad (14)$$

According to formula (13) and (14), it can be found that (i) the dissolution of the carbon steel in the anode region can accelerate the formation of the corrosion products, (ii) the oxygen reduction reaction in the cathode region produces OH– and the pH value of the steel surface is changed and (iii) the compounds of Fe^{2+} and Fe^{3+} (such as sulfate ($FeSO_4$), chloride ($FeCl_3$), iron hydroxide [$Fe(OH)_2$, $Fe(OH)_3$] and oxides (Fe_3O_4, γ-Fe_2O_3)) are generated on the steel surface.

When the proposed PASPG2 is added, the above-mentioned corrosion process will be changed. First, PASPG2 molecules are adsorbed on the steel surface because of the electrostatic action, which has been proved by the PZC tests. The adsorption process can be understood by the replacement reaction between the water molecules and PASG2. The equation for the replacement reaction is the following [Chen et al. 2019]:

$$PA - T_{(so)} + YH_2O_{(ad)} \rightarrow PA - T_{(ad)} + H_2O_{(so)} \quad (15)$$

where PA-T(so) and PA-T(ad), represent the PASG2 in the solution and adsorbed on the steel surface, respectively and Y denotes the number of water molecules replaced by PASPG2.

Subsequently, the chemical adsorption process of PASPG2 takes place in the anode region, which can be understood by the fact that the lone electron pair in the (N, O)-atoms of PASPG2 and the empty d orbital of the iron atom were combined and formed the complex. Therefore, the reaction equation in the anode region was changed from formula (13) to (15) after adding PASPG2:

$$Fe^{2+} + PA - T_{(ad)} \rightarrow [Fe \cdots PA - T]^{2+}{}_{(ad)} \quad (16)$$

where $[Fe...PA\text{-}T]^{2+}{}_{(ad)}$ represents the complex on the steel surface. From formula (16), it can also be found that the dense protective film cannot be generated when the concentration of PASPG2 is low. Therefore, the concentration of PASPG2 needs to be increased for practical applications to combine the PASPG2 molecule and iron ion to form a sufficient complex for protecting the carbon steel.

The process of corrosion inhibition is depicted in Fig. 18. Particularly, without the inhibitor, the surface of the carbon steel is covered by the water molecules and corrosion media, such as chloride ions and a small amount of oxygen molecules. However, after PASPG2 was added, its molecules will be adsorbed on the steel surface and isolate the carbon steel from the water molecules, chloride ions, and oxygen molecules. Besides, due to the advantages of PAPSG2, such as large molecular weight and a big number of polar groups, the dense protective film can be generated on the surface of the carbon steel. As was described in the electrochemical impedance diagrams (Fig. 12), a protective film was formed on the surface of the carbon steel electrode, which increased the resistance to be eroded, and thus protected the carbon steel.

4. Conclusion

1. A new inhibitor called PASPG was synthesized by the polymerization of PSI and Gly and characterized by FTIR, 1H NMR, and TGA techniques.

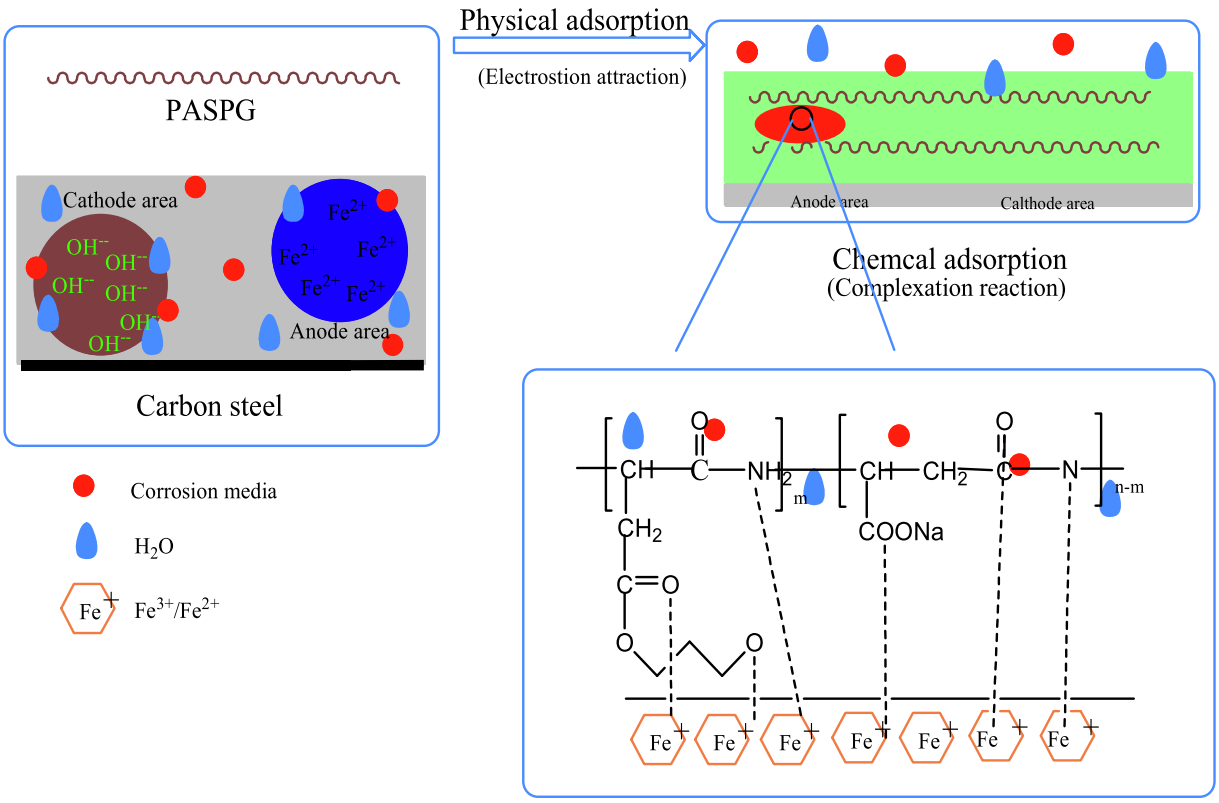

Fig. 18 The schematic diagram of the corrosion inhibition process of PASPG2.

2. The static inhibition method was used to acquire the scale inhibition efficiency against $CaCO_3$ (94.6 %) and $CaSO_4$ (95.1 %). Under the same experimental conditions, the scale inhibition efficiency of PASPG was obviously better than that of PASP.

The SEM and FTIR experiments revealed that PASPG can effectively inhibit the growth of the crystals and distort the crystal lattice of $CaCO_3$ ($CaSO_4$).

4. PASPG as a green inhibitor exhibited 85.17 % maximum corrosion inhibition efficiency. The adsorption of PASPG on carbon steel surface obeyed Langmuir adsorption isotherm. Besides, it was proved that a protective film was formed on the surface of carbon steel by PASPG's adsorption through characterization, by carrying out EIS and SEM measurements, which increased the resistance to be eroded. Thus, the surface of carbon steel was effectively protected.

In conclusion, in this work sufficient theoretical support for the proposed PASPG was provided and its potential in the field of scale and corrosion inhibition was demonstrated.

5. Author agreement

All authors have approved of the publication of this paper. We declare that the paper is the original research.

Declaration of Competing Interest

The authors declare that they have no known competing financial interests or personal relationships that could have appeared to influence the work reported in this paper.

Acknowledgment

This work was financially supported by Natural Science Foundation of Hebei Province of China (D2022105004), the Foundation of Tangshan Normal University of China (2022C42) and the Foundation of phased achievement of the key cultivation project of Tangshan Normal University of China (ZDPY07, ZDPY05).

References

Abd-El-Khalek, D.E., Abd-El-Nabey, B.A., Abdel-kawi, M.A., et al, 2016. Investigation of a novel environmentally friendly inhibitor for calcium carbonate scaling in cooling water. Desalin. Water Treat. 57, 1–7. https://doi.org/10.1080/19443994.2014.987174.

Al-Roomi, Y.M., Hussain, K.F., 2015. Application and evaluation of novel acrylic based $CaSO_4$ inhibitors for pipes. Desalin. 355, 33–44. https://doi.org/10.1016/j.desal.2014.10.010.

Amin M. A., Ibrahim M. M.. 2011. Corrosion and corrosion control of mild steel in concentrated H2SO4 solutions by a newly synthesized glycine derivative. Corros. Sci., 53,873-885 https://doi: 10.1016/j.corsci.2010.10.022.

Bukuaghangin O., Sanni O., Kapur N. 2016. Kinetics study of barium sulphate surface scaling and inhibition with a once-through flow system. J. Pet. Sci. Eng., 147, 699–706. https://doi: 10.1016/ j. petrol.2016.09.035.

Chai C.X., Xu Y,H., Xu Y., et al. 2020. Dopamine-modified polyaspartic acid as a green corrosion inhibitor for mild steel in acid solution. Eur. Polym. J., 137, 109946. https://doi.org/10.1016/ j.eurpolymj.2020.109946.

Chaussemier, M., Pourmohtasham, E., Gelus, D., et al, 2015. State of art of natural inhibitors of calcium carbonate scaling. a review article. Desalin. 356, 47–55. https://doi.org/10.1016/j.desal.2014.10.014.

Chen, Y., Chen, X.S., Liang, Y.N., 2020. Synthesis of polyaspartic acid/graphene oxide grafted copolymer and evaluation of scale inhibition and dispersion performance. Diamond Relat. Mater. 108. https://doi.org/10.1016/j.diamond.2020.107949.

Chen J.X. , Xu L.H., Han J., et al. 2015. Synthesis of modified polyaspartic acid and evaluation of its scale inhibition and dispersion capacity. Desalin., 358:42–48. http://dx.doi.org/10.1016/ j.desal.2014.11.010.

Chen, J.X., Wang, C., Han, J., et al, 2019. Corrosion inhibition performance of threonine-modified polyaspartic acid for carbon steel in simulated cooling water. J. Appl. Polym. 47242, 1–12. https://doi.org/10.1002/app.47242.

Dehghani, A., Bahlakeh, G., Ramezanzadeh, B., et al, 2019. Electronic/atomic level fundamental theoretical evaluations combined with electrochemical/surface examinations of Tamarindus indiaca aqueous extract as a new green inhibitor for mild steel in acidic solution (HCl 1 M). J. Taiwan Inst. Chem. E. 102, 349–377. https://doi.org/10.1016/j.jtice.2019.05.006.

EL-Haddad M. N.. 2014. Hydroxyethylcellulose used as an eco-friendly inhibitor for 1018 c-steel corrosion in 3.5% NaCl solution. Carbohydr. Polym., 112,595-602. https://doi: 10.1016/ j.carbpol.2014.06.032.

Farag, A.A., Hegazy, M.A., 2013. Synergistic inhibition effect of potassium iodide and novel Schiff bases on X65 steel corrosion in 0.5 M H_2SO_4. Corros. Sci. 74, 168–177. https://doi.org/10.1016/ j.corsci.2013.04.039.

Fu L.P., Lv J. , Zhou L., et al. 2020. Study on corrosion and scale inhibition mechanism of polyaspartic acid grafted b-cyclodextrin. Mater. Lett., 264 :127276. https://doi.org/ 10.1016/ j.matlet.2019.127276.

Fu, C.G., Zhou, Y.M., Xie, H.T., et al, 2010. Double-hydrophilic block copolymers as precipitation inhibitors for calcium phosphate and iron(III). Ind. Eng. Chem. Res. 49, 8920–8926. https://doi.org/ 10.1021/ie100395z.

Gao Y,H., Fan L,H., Ward L., et al. 2015. Synthesis of polyaspartic acid derivative and evaluation of its corrosion and scale inhibition performance in seawater utilization. Desalin., 365:220–226. https://doi.org/10.1016/j.desal.2015.03.006Get rights and content.

Ge, J.J., Yang, W., Zhang, G.C., 2016. Investigation of scale inhibition mechanisms based on the effect of HEDP on surface charge of $CaCO_3$. Tenside Surf. Deterg. 53, 29–36. https://doi.org/10.3139/ 113.110407.

Geethanjali, R., Sabirneeza, A.A.F., Subhashini, S., 2014. Water-Soluble and biodegradable pectin- grafted polyacrylamide and pectin-grafted polyacrylic acid: electrochemical investigation of corrosion-inhibition behaviour on mild steel in 3.5% NaCl media. Indian J. Mater. Sci. 4, 1–9. https://doi.org/10.1155/2014/356075.

Guo X,Y., Joy J. S. C. , Cheng Y.M., et al. 2021. Scale Inhibitors for Industrial Circulating Water Systems:A Review. J.Wat. Chemi. Techn., 43(6):517–525. https://doi.org/ 10.3103/S 1063455X21060102.

Huang H.H., Yao Q., Jiao Q. , et al... 2019. Polyepoxysuccinic acid with hyper-branched structure as an environmentally friendly scale inhibitor and its scale inhibition mechanism. JSCS, J. Saudi Chem. Soc.. 23(1): 61-74. https://doi:10.1016/j.jscs.2018.04.003.

Ketrane, R., Saidani, B., Gil, O., et al, 2009. Efficiency of five scale inhibitors on calcium carbonate precipitation from hard water: effect of temperature and concentration. Desalin. 249, 1397–1404. https://doi.org/10.1016/j.desal.2009.06.013.

Liao, B.K, Luo, Z.G., Wan, S., et al, 2023. Insight into The Anti-corrosion Performance of Acanthopanax Senticosus Leaf Extract as Eco-friendly Corrosion Inhibitor for Carbon Steel in Acidic Medium. J. Indus. Engin. Chemis 117, 238–246. https://doi.org/ 10.1016/j.jiec.2022.10.010.

Liu, X.H., Wang, W.J., Tong, X.J., 2014. Study of corrosion and scale inhibition of polyepoxysuccinic acid derivative. Asian J. Chem. 26 (22), 7716–7720. https://doi.org/10.14233/ajchem.2014.17659.

Meng, Q.W., Chen, D.Z., Yue, L.W., et al, 2007. Hyperbranched polyesters with carboxylic or sulfonic acid functional groups for crystallizationmodification of $CaCO_3$. Macromol. Chem. Phys. 208, 474–484. https://doi.org/10.1002/macp.200600466.

Migahed, M.A., Rashwan, S.M., Kamel, M.M., et al, 2016. Synthesis, characterization of polyaspartic acid-glycine adduct and evaluation of their performance as scale and corrosion inhibitor in desalination water plants. J. Mol. Liq. 224, 849–858. https://doi.org/ 10.1016/j.molliq.2016.10.091.

Mourya, P., Banerjee, S., Singh, M.M., 2014. Corrosion inhibition of mild steel in acidic solution by Tagetes erecta (Marigold flower) extract as a green inhibitor. Corros. Sci. 85, 352–363. https://doi.org/10.1016/j.corsci.2014.04.036.

Naka, K., 2003. Effect of dendrimers on the crystallization of $CaCO_3$ in aqueous solution. Top. Curr. Chem. 228, 141–158. https://doi.org/10.1007/b11009.

Nan, Z.D., Yang, Q.Q., Chen, Z.Y., 2010. Novel morphologies and phase transformation of $CaCO_3$ crystals formed in CDS and urea aqueous solution. J. Crystal Growth 312, 705–713. https://doi.org/ 10.1016/j.jcrysgro.2009.12.044.

Nayunigari, M.K., Maity, A., Agarwal, S., et al, 2016. Curcumin–malic acid based green copolymers for control of scale and microbiological growth applications in industrial cooling water treatment. J. Mol. Liq. 214, 400–410. https://doi.org/10.1016/ j.molliq.2015.11.034.

Obota I.B., , Onyeachub I. B., Kumar A.M.. 2017. Sodium alginate: A promising biopolymer for corrosion protection of API X60 high strength carbon steel in saline medium. Carbohydr. Polym., 178, 200-208. https://doi: 10.1016/j.carbpol.2017.09.049.

Qiang, Y., Li, H., Lan, X., 2020. Self-assembling anchored film basing on two tetrazole derivatives for application to protect copper in sulfuric acid environment. J. Mater. Sci. Technol. 52, 63–71. https://doi.org/10.1016/j.jmst.2020.04.005.

Qiang, Y., Guo, L., Li, H., et al, 2021. Fabrication of environmentally friendly Losartan potassium film for corrosion inhibition of mild steel in HCl medium. Chem. Eng. J. 406,. https://doi.org/10.1016/j.cej.2020.126863 126863.

Shi, S., Li, D., Chai, C., et al, 2018. Synthesis of a polyaspartic acid/4-(2-ami-noethyl) morpholine graft copolymer and evaluation of its scale and corrosion inhibition performance. Polym. Adv. Technol. 29, 2838–2847. https://doi.org/10.1002/pat.4406.

Shi, S.C., Zhao, X.W., Qian, W., et al, 2016. Synthesis and evaluation of polyaspartic acid/furfurylamine graft copolymer as scale and corrosion inhibitor. RSC Adv. 6, 102406–102412. https://doi.org/ 10.1039/C6RA22048G.

Solomon M M , Umoren S A , Quraishi M A , et al. 2019. Myristic acid based imidazoline derivative as effective corrosion inhibitor for steel in 15% HCl medium. J. Colloid. Interf. Sci.,551: 47–60. https://doi:10.1016/j.jcis.2019.05.004.

Sun X.Y., Zhang J,P., Yin C.X., et al. 2015. Poly(aspartic acid)–tryptophan grafted copolymer and its scale-inhibition performance. J. Appl. Polym. Sci, . 132(45): 42739. https://doi.org/ 10.1002/ app.42739.

Tan B.C., Zhang S,T. , Cao X,L. et al. 2022. Insight into the anti-corrosion performance of two food flavors as eco-friendly and ultra-high performance inhibitors for copper in sulfuric acid medium. J. Colloid Interface Sci., 609: 838–851. https:// doi.org/ 10.1016/j.jcis.2021.11.085.

Tan, B.C., Zhang, S., Qiang, Y., et al, 2020. Experimental and theoretical studies on the inhibition properties of three diphenyl disulfide derivatives on copper corrosion in acid medium. J. Mol. Liq. 298,. https://doi.org/10.1016/j.molliq.2019.111975 111975.

Tan, B.C., He, J.H., Zhang, S.T., et al, 2021. Insight into anti-corrosion nature of Betel leaves water extracts as the novel and eco-friendly inhibitors. J. Colloid Interface Sci. 585, 287–301. https://doi.org/10.1016/j.jcis.2020.11.059.

Tan B.C., Lan W. , Zhang S.t., et al. 2022. Passiflora edulia Sims leaves Extract as renewable and degradable inhibitor for copper in sulfuric acid solution. Colloids Surf., A. https://doi.org/ 10.1016/ j.colsurfa. 2022.128892.

Wan, S., Wei, H.X., Quan, R.X., et al, 2022. Soybean extract firstly used as a green corrosion inhibitor with high efficacy and yield for carbon steel in acidic medium. Ind. Crops Prod. 187,. https://doi.org/10.1016/j.indcrop.2022.115354 115354.

Wang, C., Chen, J.X., Han, J., et al, 2019. Enhanced corrosion inhibition performance of novel modified polyaspartic acid on carbon steel in HCl solution. J. Alloys Compd. 771 (15), 736–746. https://doi.org/10.1016/j.jallcom.2018.08.031.

Wang, H.F., Gao, M.D., Guo, Y., et al, 2016. A natural extract of tobacco rob as scale and corrosion inhibitor in artificial seawater. Desalin. 398, 198–207. https://doi.org/10.1016/j. desal.2016.07.035.

Yang, L., Yang, W.Z., Xu, B., et al, 2017. Synthesis and scale inhibition performance of a novel environmental friendly and hydrophilic terpolymer inhibitor. Desalin. 416, 166–174. https://doi.org/10.1016/j.desal.2017.05.010.

Zeino, A., Abdulazeez, I., Khaled, M., et al, 2018. Mechanistic study of polyaspartic acid (PASP) as eco-friendly corrosion inhibitor on mild steel in 3% NaCl aerated solution. J. Mol. Liq. 250, 50–62. https://doi.org/10.1016/j.molliq.2017.11.160.

Zeng, Y.X., Kang, L., Wu, Y., et al, 2022. Melamine modified carbon dots as high effective corrosion inhibitor for Q235 carbon steel in neutral 3.5 wt% NaCl solution. J. Mol. Liq. 349,. https://doi.org/10.1016/j.molliq.2021.118108 118108.

Zhang, S.P., Qu, H.J., Yang, Z., et al, 2017. Scale inhibition performance and mechanism of sulfamic/amino acids modified polyaspartic acid against calcium sulfate. Desalin. 419, 152–159. https://doi.org/10.1016/j.desal.2017.06.016.

Zhang, Y., Yin, H.Q., Zhang, Q.S., et al, 2016. Synthesis and characterization of novel polyaspartic acid/urea graft copolymer with acylamino group and its scale inhibition performance. Desalin. 395, 92–98. https://doi.org/10.1016/j.desal.2016.05.020.

Zhao, L.N., Zhou, Y.M., Yao, Q.Z., et al, 2021. Calcium scale inhibition of stimulated oilfield produced water using polyaspartic acid/aminomethanesulfonic acid. ChemistrySelect 6 (15), 3692–3701. https://doi.org/10.1002/slct.202100853.

Zhou Y.S.; Jie W.; Yan F.. 2021. Green and High Effective Scale Inhibitor Based on Ring-Opening Graft Modification of Polyaspartic Acid. Catalysts, 11(7): 802-802. https://doi.org/10.3390/catal11070802.